

Suction and Oscillatory Blowing Actuator

Gilad Arwatz[◦], Ilan Fono[♦] and Avi Seifert^{*}

School of Mechanical Engineering

Tel-Aviv University, Tel-Aviv, Israel

Abstract

Enhancing the ability to control flows in different configurations and flow conditions can lead to improved, flow-related, energy-efficient systems. Certain active flow control actuators are effective at low Mach numbers but the momentum and vorticity they provide limits their utilization to low speeds. At higher Mach numbers, robust, unsteady, effective and practical fluidic actuators are a critical, enabling technology in any flow control system, though they are largely missing. A new actuator concept, based on the combination of steady-suction and oscillatory-blowing is presented. The actuator achieves near-sonic speeds at a frequency range from 10Hz to at least 1kHz. It has no moving parts and therefore is expected to have superior effectiveness and reliability. The operating principles of the new actuator are presented along with two computational models and their experimental validation.

Nomenclature

a	acceleration, [m/s ²]
A	cross section area, [m ²]

[◦] Graduate student

[♦] Consultant

^{*} Associate Professor of Mech. Eng., seifert@eng.tau.ac.il

b	valve inlet nozzle width, [m]
c	chord, [m]
C_p	pressure coefficient
C_μ	steady blowing/suction momentum coefficient; $\equiv \frac{H\rho_a V_a^2}{\frac{1}{2}\rho_\infty c U_\infty^2}$
$\langle C_\mu \rangle$	oscillatory blowing momentum coefficient; $\equiv \frac{H\rho_j \langle V_j \rangle^2}{\frac{1}{2}\rho_\infty c U_\infty^2}$
d_c	valve control port channel width (diameter), [m]
d_{e_in}	ejector inlet nozzle width (diameter), [m]
d_{e_out}	ejector outlet width (diameter), [m]
d_t	feedback tube diameter, [m]
E	power consumption, [Watt]
f	frequency, [Hz]
F	thrust, [N]
F^+	reduced frequency; $\equiv \frac{f \cdot X_B}{U_\infty}$
g	pressure gradient, [Pa/m]
H	suction/blowing slot height, [m]
h	valve inlet nozzle height, [m]
l	valve length, [m]
L	inductance (self-excited oscillations frequency model), [kg/m ⁴]
l_c	valve control port channel length, [m]
L_e	ejector length, [m]
L_{mix}	ejector mixing chamber length, [m]
l_t	feedback tube length, [m]
M	Mach number
\dot{m}	mass flow-rate, [kg/s]
OFM	overall figure of merit $\equiv \frac{F_a^2 U_p}{W_a E}$

P	Pressure, [Pa]
P_c	control differential pressure, [Pa]
Q	volumetric flow-rate, [m ³ /s]
R	resistance (self-excited oscillations frequency model), [kg/m ⁴ s]
r	valve corner-radius, [m]
Re	Reynolds number
S_d	splitter distance, [m]
S_t	Strouhal number
t	time, [s]
T	cycle time, [s]
U	velocity, [m/s]
u	horizontal velocity, [m/s]
U_∞	free stream velocity, [m/s]
U_c	jet center velocity (jet deflection model), [m/s]
U_p	actuator peak velocity, [m/s]
v	vertical velocity, [m/s]
W	weight, [N]
X_l	control port width (jet deflection model), [m]
X_B	length of separated region, [m]
Y_l	jet deflection at valve exit (jet deflection model), [m]
γ	specific heat ratio
κ	Valve switching quality; $\equiv (Q_L / Q)$; with L the left exit
η_e	entrainment-ratio; $\equiv Q_2 / Q_1$
ρ	density, [kg/m ³]
σ	valve inlet aspect-ratio; $\equiv h / b$
τ	transport time, [s]
τ_c	control transport time (jet deflection model), [s]
τ_s	splitter transport time (jet deflection model), [s]
τ_{ac}	acoustic delay (self-excited oscillations frequency model), [s]

τ_{LR}	time constant of inductor-resistor circuit, [s]
ν	kinematic viscosity, [m ² /s]
ω	radial frequency; =2 π f, [rad/sec]

Subscripts

*	throat conditions
0	stagnation conditions
1	ejector inlet flow
2	ejector suction flow
3	ejector total flow
∞	free-stream conditions
a	actuator
back	back-pressure
blw	blowing
inlet, i	inlet conditions
out, o	output conditions
suc	suction

Acronym

2D	two-Dimensional
3D	three-Dimensional
AFC	Active Flow Control
AC	Alternating Current
BLC	Boundary Layer Control
CFD	Computational Fluid Dynamics
DC	Direct Current
FFT	Fast Fourier Transform
MEMS	Micro-Electrical Mechanical System
PIV	Particle Image Velocimetry
PSD	Power Spectral Density
RPM	Revolutions Per Minute

TAU Tel-Aviv University
UAV Unmanned Air Vehicle
ZMF Zero-Mass-Flux

1. Introduction

Background and motivation

The development of techniques for expanding the ability to control flows in a wide variety of configurations and flow conditions can lead to greatly improved flow-related systems. Probably the most common flow control application is the control of incompressible boundary layer separation, which augments the performance of flight vehicles in aspects such as increased lift, enhanced stall-margin, drag reduction, noise and vibration attenuation. The control of incompressible boundary layer separation can also enable shorter inlets and diffusers as well as thrust vectoring. It has been shown that active flow control (AFC) can be effective in compressible flows [1,2], but higher control authority (the capability to alter the flow field) or input momentum is required for boundary layer control when compared to the momentum requirements for similar incompressible applications.

The structure of the paper is as follows: First we review various actuator concepts and present the new actuator operating principles. The experimental setup is presented after the Introduction. The valve switching mechanism is explained using transfer characteristic diagrams. Two computational models that were developed are presented along with their experimental validation. Several ejector sizes and geometries and an improved small-size actuator are presented. Finally, the effectiveness of the new actuator is analyzed and compared with other actuators. Conclusions and recommendations are discussed.

Actuator concepts

AFC Actuators can be divided into two categories, based on the fluidic principle of operation: Zero-Mass-Flux (ZMF or "synthetic jet") and Mass-Flux actuators (MF, continuous or pulsed jets, steady or pulsed suction). Synthetic jets can be very effective for active flow control [3,4,5], however their main shortcoming is the magnitude of the momentum and vorticity flux they can provide, currently limited to peak velocity of about $M=0.3$. Therefore, robust, unsteady fluidic actuators** are critical enabling technology components in any successful AFC system. Many types of actuators are currently at different levels of development and application stages. A partial list and brief discussion follows.

Piezoelectric actuators (fluidic and mechanical)

Piezoelectric materials that develop mechanical strain in response to an applied electric field are suitable for AFC actuators. The use of piezoelectric materials for flow control can be divided into two categories: mechanical actuators and fluidic actuators.

Mechanical piezoelectric actuators

Examples of mechanical actuators are surface mounted piezo benders that produce significant flow disturbances over a wide range of frequencies. Surface mounted, mechanical actuators rely on the interaction with the incoming boundary-layer-shear to generate the excitation. To avoid substantial drag penalty and to minimize the aerodynamic loading on the actuator, the device is often flush-mounted to the surface [6] or mounted in a recessed shallow cavity [3]. Piezoelectric mechanical actuators usually consist of a piezoceramic material bonded to a metal plate. When AC voltage is applied to the piezoelectric material, it alternately expands and contracts, causing the metal plate to oscillate at the applied frequency.

The main advantage of these kinds of actuators is simplicity. However, because they require direct contact with the controlled flow, they produce parasite-drag and their efficiency is limited to low speeds and they are susceptible to damage.

Piezoelectric fluidic actuators

In contrast to mechanical piezoelectric actuators, fluidic actuators do not need direct interaction with the controlled external fluid. Piezoelectric fluidic actuators are cavity based Zero-Mass-Flux (ZMF, “synthetic jet”) devices, usually consisting of three elements: a pressure fluctuation generating mechanism, a cavity and a slot, connecting the cavity with the flow to be controlled. Most commonly, the cavity pressure fluctuations are generated by an oscillating piezoelectric material bonded to membranes that form at least one of the cavity walls and are driven by an electric AC signal. The AC voltage causes the membrane to oscillate at the applied frequency generating pressure oscillations that, in turn, create velocity fluctuations with zero mean through the exit slot or hole (Fig.1 [7]).

These types of fluidic actuators are very effective for active flow control applications. They have almost all the desirable characteristics of actuators: a wide bandwidth, lightweight, low power

consumption, low cost, durability and reliability. Their main shortcoming is the relatively low momentum and vorticity flux they produce. In fact, significant output is restricted to the mechanical or the Helmholtz resonance frequencies of the actuator, which are much higher than the unstable frequencies (of the base flow) to be controlled. To overcome this obstacle, Amplitude Modulation (AM) at low modulation frequencies or Burst Mode (BM or pulsed modulation) can be used [4, 5].

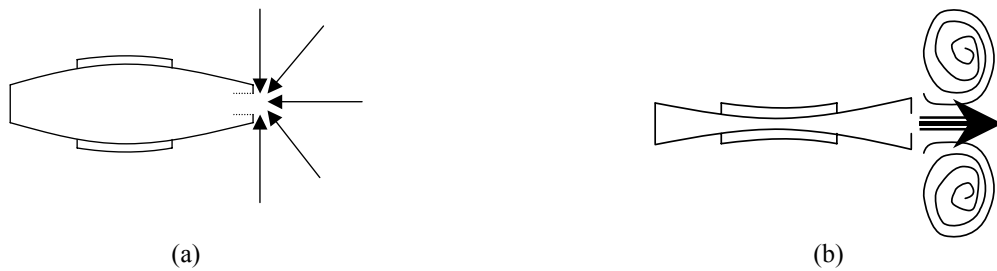


Fig.1: Schematic diagram showing the operating principle of cavity-based piezoelectric fluidic actuator.(a) Suction stage (b) blowing stage [7].

Pulsed Combustion Jet actuator

Combustion jet actuators are based on subsonic wave combustion process. They operate at a much longer time-scale than that of the wave expansion within the device. Their operation is similar to small pulsed detonation engines [8]. They consist of an inlet valve to periodically inject fuel, an igniter to initiate combustion, a tube in which the combustion takes place and an exit slot or hole (Fig.2).

Combustion jet actuators are capable of providing high impulse (7 Psi) at a wide frequency range (100Hz to 1500Hz), hence, they are a suitable solution for boundary layer separation control at high speeds [9].

The main disadvantage of these devices is the need for high temperature, exotic materials. Also, the internal combustion process consumes fuel, requires premixing, a mixing device, and adds safety concerns along with installation difficulties. The large size and heavy weight of the actuator, because they must be robust and supply a wide range of frequencies, are further drawbacks.

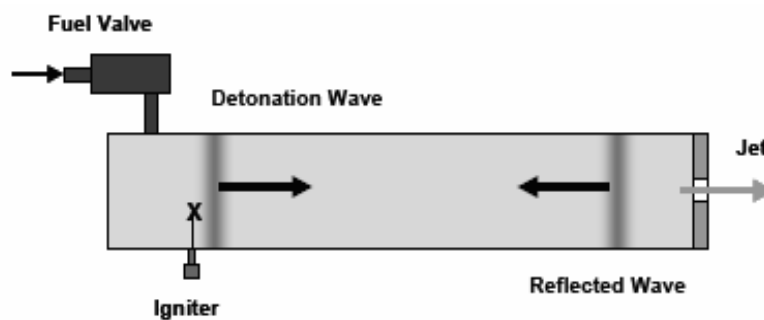


Fig.2: A simplified schematic diagram of pulsed combustion jet actuator [9].

The Hartmann tube

The Hartmann tube is a device that uses the oscillations of a shock wave to produce high intensity sound waves. The phenomenon was discovered by Julius Hartmann (1919) when using a Pitot probe in a compression region of a jet.

Gregory and Sullivan [10] describe the operating principle of the Hartmann tube, see Fig.3. Flow is exiting a nozzle on the left and entering into a resonance cavity on the right. The oscillation sequence consists of two main stages indicated in the diagram: filling the resonance cavity (Fig.3a), and discharge of flow from the cavity (Fig.3b). When the flow is released from the resonance cavity, it disperses radially with the flow from the jet, the motion of the external shock wave is driven by the periodic nature of the flow entering and exiting the resonance cavity.

The use of high intensity sound for flow control application was demonstrated in many studies, and can provide a limited control authority at low speeds [11]. Using high-amplitude, high-frequency pressure waves might also be suitable for high-speed flow control [12]. However, the receptivity of the sound waves by the separating turbulent boundary layer might be a limiting factor.

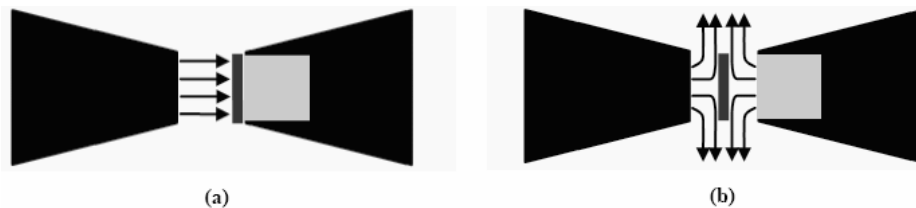


Fig.3: Conceptual drawing showing the operating mechanism of the Hartmann tube, including shock oscillation. (a) Filling of resonance cavity (b) cavity discharge [10].

Plasma actuators

The fundamental operating principle of plasma actuators is based on creating kinetic energy inside the boundary layer of an external or internal flow in order to modify its properties. Methods of plasma generation include DC, AC, RF, microwave, arc, corona, and spark electric discharge.

Labergue et al. [13] explained that for the case of a DC corona discharge established between two electrodes flush-mounted along a PolyMethyl-MethAcrylate (PMMA) surface in air at atmospheric pressure, positive ions are produced at the anode and electrons at the cathode. In their drift motion between the two electrodes under Coulomb forces, the ions exchange momentum with neutral particles and induce an airflow, called ionic wind. Most of the plasma actuators operate in a similar manner. The process also creates an intense, localized and rapid heating, causing pressure perturbations which can considerably modify the near-wall flow and fluid properties.

The amplitude of the plasma actuators depends on the supplied current and the fluid properties. Temperature has a strong effect on the actuator's performance. Plasma actuators were proven to be effective in high-speed cold jet [14] and in boundary layer control at very low speeds [15]. One of the shortcomings of plasma actuators is the need to generate high voltage at high frequency. This is accompanied by energy losses and additional weight. Another disadvantage is the sensitivity to the controlled fluid properties and environmental conditions (e.g., humidity can cause dramatic changes in the efficiency and even damage). The generation of plasma is also highly visible.

Oscillatory-blowing actuators

As mentioned, oscillatory-blowing is an effective tool to delay boundary layer separation. The general idea of oscillatory-blowing actuators is use of periodic blowing through a narrow spanwise slot or array of holes to enhance shear-layer mixing and transfer high-momentum fluid from outside the shear-layer to the wall region and thus prevent boundary layer separation. There are many kinds of oscillatory blowing actuators; most of them use a pressurized source and some kind of oscillatory valve (e.g., solenoid valve, rotating valve with sets of holes that periodically go in and out of alignment) a cavity, and an exit slot.

One of the oscillatory-blowing actuators' shortcomings is the need to use piping to connect the various components. These piping connections could produce many resonant frequencies and result in additional pressure drop. Most oscillatory-blowing devices generate a significant pressure loss, and therefore, they have low overall system efficiency.

The main advantage of the oscillatory-blowing actuators is the large momentum they can deliver and the option of having several high-amplitude operating frequencies. However, oscillatory-blowing valves also require a pressure source. The pressure source can be bleed air from the power-plant of the controlled vehicle or some kind of compressor, or even a pressurized vessel. In any configuration, the system is relatively large, complex, heavy, and energy consuming.

Fluidic amplifiers

Recently, renewed interest has been focused on the well-known concept of bi-stable fluidic oscillators [20], as an alternative to "synthetic jets". In a recent study, Tesar et al [16] use a fluidic amplifier to switch an inlet flow to two exits. They use the length of a feedback tube (with a

minimum length of 1m) as the primary frequency control mechanism. The feedback tubes are each connected to one exit port. This is an inherent shortcoming due to the associated transport delay, increasing the minimum switching time. They do not investigate the effect of exit resistance, nor do they present the exit velocities. They do not present a physical nor mathematical model for the valve operation. In this paper, we present a new, patented flow control valve [17] (priority date from October 2003, patent submitted in September 2004) that combines an ejector (also referred to as a “jet-pump”) and a bi-stable fluidic-amplifier to generate both steady-suction and pulsed-blowing using a miniature, no-moving-parts device. Both AFC methods are known to be very effective, but have never been used before in close proximity and were never generated before by one simple, effective, and robust device. Two models for the switching mechanism and for the oscillation frequency are provided. Several methods for altering and controlling the frequency are suggested and the effects of loading the suction and exit ports are discussed. The exit velocities as well as the switching characteristics of the valves are measured. The actuator is now being applied for boundary layer separation control of a bluff-body. Those results are presented in a separate publication.

Operation principle of the new actuator

The new device combines steady-suction and oscillatory-blowing, both proven to be very effective AFC tools. The actuator is a combination of an ejector and a bi-stable fluidic amplifier (Fig.4).

The ejector (Fig.4a) is a simple fluidic device based on Bernoulli’s law. When a jet stream is ejected into a bigger conduit it creates low pressure region around it due to entrainment. The cavity behind the jet is open to the free-atmosphere, or to a lower pressure environment (such as the upper surface of an airfoil). As a result, the pressure gradient around the internal jet will cause the external air to be sucked into the cavity [18,19]. The common use of ejectors is to increase the flow-rate. However, if the fluid is drawn from an aerodynamic surface, a suction flow is created across the aerodynamic surface through slots or holes. The bi-stable fluidic amplifier is based on the principle of wall-attachment [20]; when a fluid jet is flowing in the proximity of a wall, a low-pressure region is formed between the jet and the wall. The low pressure draws the jet towards the wall, deflecting the jet until it adheres to the. In the case of two near and symmetric walls (Fig.4b), the jet will randomly re-attach to either wall. If an appropriate pressure gradient is introduced between the control ports (Fig.4b), the jet will detach from one wall and re-attach to the opposite wall. By connecting the control ports by a tube, the bi-stable fluidic amplifier can self-oscillate and serve as a switching-

valve. In this configuration, the oscillation frequency is related to the tube length and diameter, the speed-of-sound in the tube, the flow-resistance of the control ports and the flow-rate through the device [21,22].

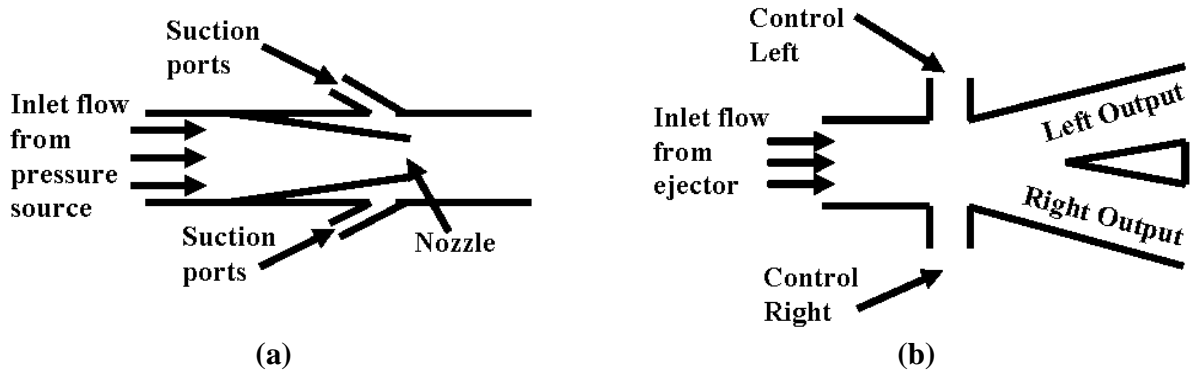


Fig.4: A schematic rendering of the SaOB actuator: (a) ejector (b) switching valve.

2. Experimental setup

Three sets of actuators of different sizes were built to examine the actuators' performance and validate the models. First, the feasibility of using the concept presented in Figure 4 as flow control actuator was tested with a large-size model. Based on this proof-of-concept, several medium-size actuators were fabricated in order to determine geometry effects on performance. A small-size actuator was fabricated using a successful geometry. The small-size actuator is suitable for AFC applications, where the aerodynamic scale (e.g., length of separated region) is of typical dimensions of 10–100cm at low subsonic to near-sonic Mach numbers.

Figure 5 presents a schematic diagram, top-view, of the generic switching-valve used in the present study. Table 1 summarizes all valve dimensions, given in terms of the nozzle width (b).

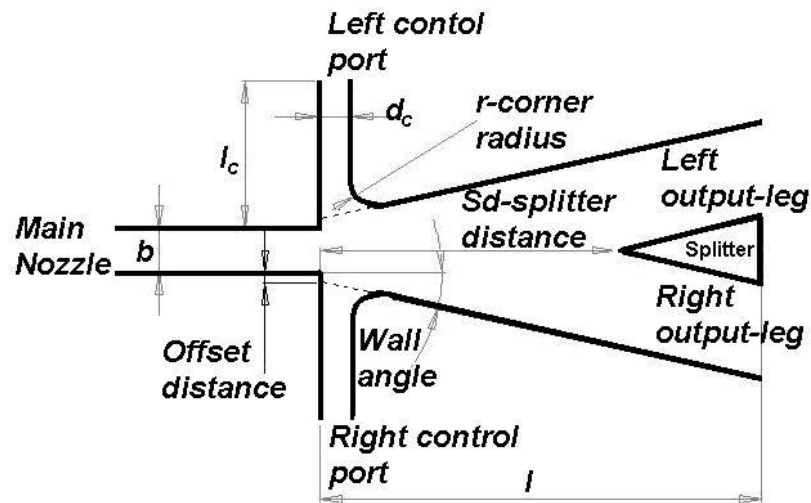


Fig.5 : Generic geometry of the switching valve. All dimensions are subsequently scaled by the main nozzle width, b .

Parameters / valve number	Large-size valve	Medium-size valve				Small-size valve	
	#1	#1	#2	#3	#4	#1	#2
Inlet nozzle width (b), mm	10	3	3	3	3	1.5	1.5
Valve depth (h/b)	0.8	1.5	1.5	1.5	1.5	1.5	3.3
Valve length (l/b)	7	10	10	10	10	10	10
Control channel length (l_c/b)	4.5	4.5	4.5	4.5	4.5	4.5	4.5
Control channel width (d_c/b)	0.8 Φ	0.75	0.75	0.75	0.75	0.75	0.75
Corner-radius (r/b)	0	1	1	0.5	0	1.0	1.0
Splitter distance (S_d/b)	1-6	6	8	8	8	8.0	8.0
Wall angle	14°	12°	12°	12°	12°	12°	12°

Table 1: Switching valve dimensions, in units of b , according to Fig. 5.

Large-size valve (Table 1 and Fig. 5)

The main nozzle jet has a rectangular cross section with width, b , and height (or depth), h . The control ports are of a circular cross-section with diameter, d_c . The large-size valve has sharp corners

($r=0$). The splitter was attached to the device using two pins. By relocating the splitter, it was possible to control the splitter distance, S_d .

Medium-size valve (Table 1 and Fig. 5)

Four medium-size valves were fabricated according to Drzewiecki's design guidelines [23]. All valves have the same inlet width and shape (inclined); only the splitter distance or the corner-radius is different.

Small-size valve (Table 1 and Fig. 5)

Two small-size valves were fabricated according to Drzewiecki's guidelines [23]. The two valves have the same geometry except for the valve depth and the inlet nozzle shape.

2.1. Ejectors

Large-size ejector

Figure 6 shows a cross section view of the large-size ejector. All dimensions are in terms of the switching valve nozzle width (b). The large-size prototype of the ejector has a cylindrical mixing chamber. The total length of the ejector, L_e , is $9b$. The mixing chamber length, L_{mix} , is $5.4b$. The inlet jet nozzle has a circular cross section with a constant diameter, d_{e_in} , of $0.27b$. The outlet has a circular cross-section with diameter, d_{e_out} , of $1b$. A total of 12 circular suction holes with a diameter of $0.25b$ each are situated at uniform distribution (i.e., every 30°) around the entrance to the mixing chamber behind the nozzle exit. The suction holes are drilled at an angle of 30° with respect to the ejector inlet flow direction.

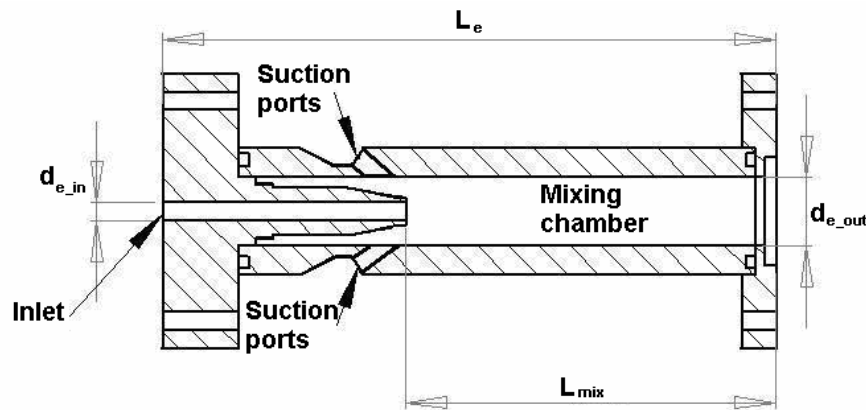


Fig.6: Large-size, axis-symmetric, ejector cross section.

Medium-size ejector A medium-size ejector was fabricated and connected to the medium-size valves. The shape of the ejector is similar to that of the large-size ejector, as shown in Fig.6.

The total length of the ejector, L_e , is $16.67b$. The mixing chamber length, L_{mix} , is $12.3b$. The inlet has a circular cross section with a constant diameter, $d_{e_{in}}$, of $0.6b$; the outlet has a circular cross section with diameter, $d_{e_{out}}$, of $2b$. The suction ports consist of 6 circular holes with diameter of $0.6b$.

Small-size ejector

Four small-size ejectors were fabricated and combined with the small-scale switching valves. All ejectors have the same dimensions except for the inlet nozzle and depth. Two ejectors were fabricated with a converging inlet nozzle and two with converging-diverging inlet nozzle. The dimensions of the ejectors are presented in Fig.7a while the nozzles' dimensions are presented in Fig.7b and Fig.7c. The two ejectors, with the converging inlet nozzle, were 6mm in depth and the nozzle depths were 0.6mm and 1.2mm, respectively. The two ejectors with the converging-diverging inlet nozzle were 5 mm in depth, and the inlet nozzle depths were 1.2mm and 1.8mm, respectively.

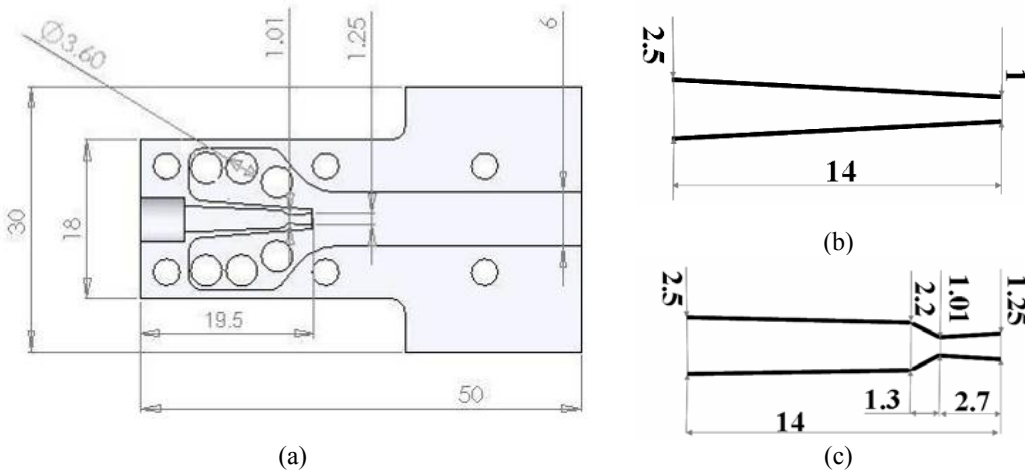


Fig.7: Small-scale ejectors (a) overall ejector dimensions, with six holes of 3.6mm diameter being the suction holes (b) converging inlet nozzle (c) converging-diverging inlet nozzle. All dimensions in millimeters.

Steady and unsteady pressures, flow-rates, velocities and frequencies were measured. More details on the experimental setup can be found in [24]. Figure 8 shows a schematic description of the experimental arrangement. Compressed shop-air was fed into the actuators' inlet by a computer controlled pressure regulator. An orifice flow-meter was placed at different positions, depending on

the experimental requirements. Steady and unsteady pressures were measured at several locations, as shown in Fig.8. The unsteady pressure signals were low-pass filtered using a Butterworth filter (cut-off frequency, $f_c=10$ kHz), amplified, and together with all the other signals, were acquired and digitized at a typical sampling rate of 25 kHz and sampling time of several seconds using a 12-bit A/D converter. The signals were ensemble-averaged in order to remove random noise and the turbulent fluctuations from the signals. The synchronization signal was the low-pass-filtered differential pressure between the control ports (input, marked ΔP on Fig.8).

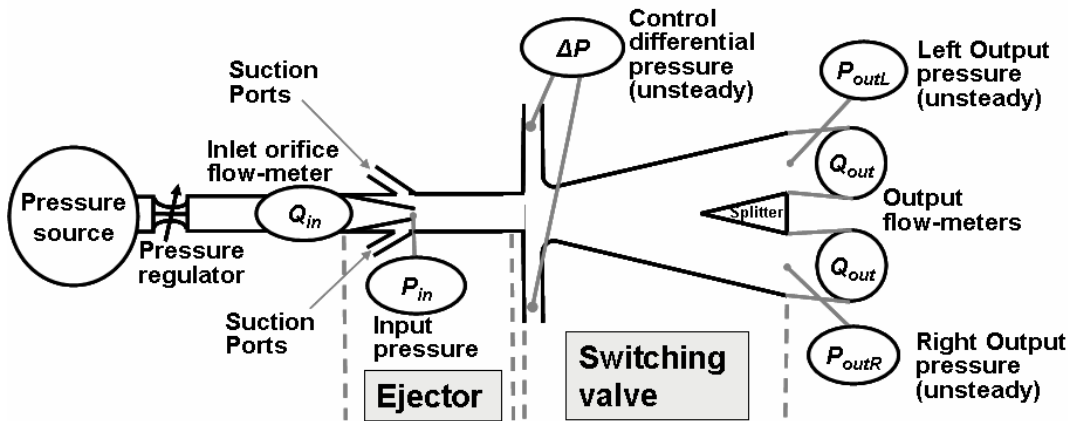


Fig.8: Actuator (ejector and switching valve) geometry and experimental setup.

2.2. Switching valve transfer characteristics

As mentioned, the valve can self-oscillate by connecting the two control ports with a tube (termed hereafter "feedback tube").

Significant insight can be gained into the valve switching mechanism by the examination of the valve transfer characteristic. The transfer characteristic diagram presented in Fig.9 describes conceptual characteristics of the valve operation. On the left side of Fig.9, the input and output signals vs. time are presented; on the right side, the transfer characteristics diagram (output vs. input) is shown. The input signal is the differential pressure between the control ports (ΔP_c , static pressures). The output signal is the differential pressure between the outlets (ΔP_o , total pressures) that is directly related to the jet deflection at the valve exit.

To explain the valve transfer characteristics, it is useful to look at key points in the input and output signals vs. time (Fig.9a) and the corresponding points on the transfer characteristic curves (Fig.9b). In the following paragraphs, we attempt to clarify the operating mechanism of the switching valve, according to the nomenclature of Fig.9a and Fig.9b.

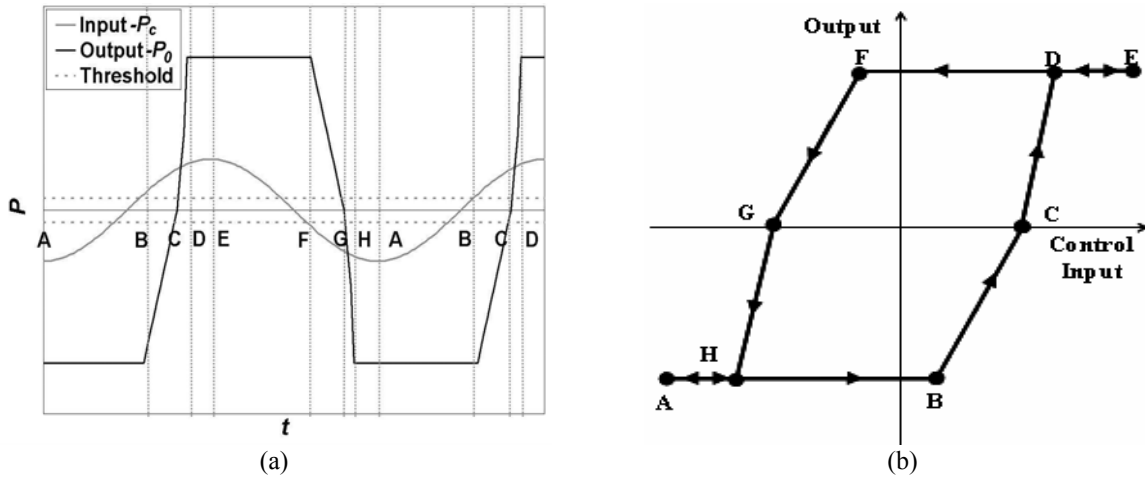


Fig.9: Predicted valve switching characteristics (a) input and output signals vs. time (b) transfer characteristics: output vs. input.

A-B: The input signal (the differential control pressure) is increasing from its minimal pressure to the positive threshold pressure. The jet remains attached to the lower wall (in the orientation of Fig.8). As long as the input pressure is negative, the jet is being pulled to the lower wall by the wall-attachment effect and by the control pressure. When the input becomes positive, the control pressure pulls the jet to the upper wall but the wall-attachment effect still pulls it to the lower wall. The jet remains attached to the lower wall until the control pressure increases above a certain threshold level (a minimum control pressure is required to switch the jet, to be discussed and modeled later).

B-C: As the input control pressure increases above the positive threshold, the jet separates from the lower wall and moves upwards. The jet is pulled up by the control pressure and is pulled down by the diminishing wall-attachment effect. The result is a slow deflection of the jet towards the upper wall. The output signal increases from its minimum to zero.

C-D: The jet passes the center of the valve (zero), the wall-attachment force is changing direction and pulls the jet towards the upper wall. At this stage, the jet is being pulled-up by the control pressure and by the wall-attachment effect. The result is a rapid deflection of the jet towards the upper wall. The output signal rises from zero to the maximum. The jet switching is complete.

D-E: Since the jet is already attached to the upper wall, the output remains constant while the input is rising to the maximum. In terms of the control process, the implication is that the pressure gradient can be relaxed or the frequency can be further increased.

Segments **E-F-G-H-A** are similar to segments **A-B-C-D-E** but in the opposite direction.

The preceding description is for one cycle. When a feedback tube is connected between the two control ports and ΔPc is supercritical, the valve will oscillate, switching the jet from side to side. The self-oscillation mechanism assumed is that the low pressure created by the flow acceleration due to the jet-turning at one control port propagates through the tube to the other control port. When the pressure difference between the two control ports passes the threshold, it causes the jet to switch. This process repeats itself in the other direction and therefore the jet self-oscillates.

2.3. Jet deflection model

Overview

A simple model for describing the operation of the switching valve was developed, relying on the results of the preliminary experimental study. The model is based on analysis of the jet motion between two inclined walls due to a transverse pressure gradient between the control ports. The model follows the analysis of Kirshner and Katz [25], describing the effect of a transverse control pressure gradient on a free-jet. The main additions to the switching valve model are the boundary conditions (walls and splitter) and the wall-attachment effect.

The primary model assumptions are:

- Entire mass of jet is concentrated at the jet centerline
- Fluid is incompressible and inviscid.
- Jet axial velocity is constant (no entrainment or spreading).
- Transverse pressure gradient is uniform in the control ports region.

The model is based on the simple idea of fluid-elements flowing from the inlet nozzle to the valve outlet. When a fluid-element reaches the control ports, it experiences transverse acceleration due to the control-pressure gradient. This acceleration integrates to change the transverse velocity, which causes the fluid element to deviate from the device center-line. A “no-cross” boundary condition is applied at the walls and the splitter. Since the jet velocity profile is fairly uniform in the control region, we assume that the interaction of a fluid element with other elements can be neglected. Therefore, we restrict the discussion to the motion of the jet axis and set $u=U_c$, with U_c being the jet velocity that is assumed unchanged throughout.

We describe the dynamics of a fluid element at a transverse position, Y_o , from the jet axis, as shown in Fig.10. A transverse pressure gradient, $dp/dy = -g(x,t)$, initiated at $t = 0$, exerts a force on the fluid element and accelerates it such that:

$$\frac{d^2 y}{dt^2} = \frac{g(x,t)}{\rho} \quad (1)$$

To numerically solve (1), the basic equations of motion were used. Fig.10 shows the physical configuration of transverse pressure gradient applied between the two control ports. The pressure gradient acts on the jet, only in the control region, i.e., from $x = 0$ to $x = X_l$. Three transport times can be defined: 1) the axial transport time (the convection time from the switching valve inlet to the valve exit): $\tau = \int_0^l \frac{dx}{U_c}$; 2) the control transport time: $\tau_c = \int_0^{x_1} \frac{dx}{U_c}$; and 3) the splitter transport time:

$$\tau_s = \int_0^{S_d} \frac{dx}{U_c} \quad (\text{where } S_d \text{ is the distance between the jet exit to the splitter, see Fig.11). \text{ All integrals}$$

begin from the switching valve inlet (the termination of the constant width duct in Figs. 10 and 11).

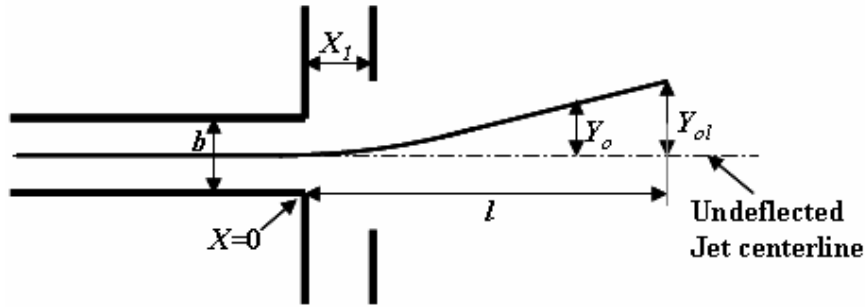


Fig.10: Jet fluid elements (shown as a line) under the effect of a transverse pressure gradient.

We further assume that the oscillatory control-pressure gradient acting on the jet is of uniform magnitude between $x = 0$ and X_l and is *zero* between X_l and l at any time. It depends on time and space in the following manner:

$$\begin{aligned} g(x,t) &= A \cos(wt) & 0 \leq x \leq x_1 \\ g(x,t) &= 0 & x_1 \leq x \leq l \end{aligned} \quad (2)$$

Where A is constant and $w = 2\pi f$ is the angular velocity.

The actual switching-valve has inclined walls and a splitter between the two exits (Fig.11). These were added to the simulation as “no-cross” boundary conditions.

Minimum switching pressure model

The minimum switching pressure, defined as the smallest pressure gradient that will flip the jet from one side to the other, will now be modeled. The model assumptions (mentioned at the beginning of Section 2.3), the simplified equations of motion (1) and the boundary and initial conditions (2) will be used. When a fluid element flows along one side of the inlet nozzle (dashed line in Fig.11) and reaches the control region, a pressure gradient will cause the fluid element to accelerate in the transverse direction, deflecting the fluid element from its original path. After a fluid element exits the control region, it will continue moving in a straight line (the current analysis ignores the wall-attachment effect, assuming that the wall-attachment pressure is negligible compared to the control pressure). If a fluid element path brings it to the opposite side of the splitter, deflecting the fluid element by at least the splitter height ($b/2$), the control pressure is considered to be large enough to cause *full switching* and is defined as the minimum switching pressure.

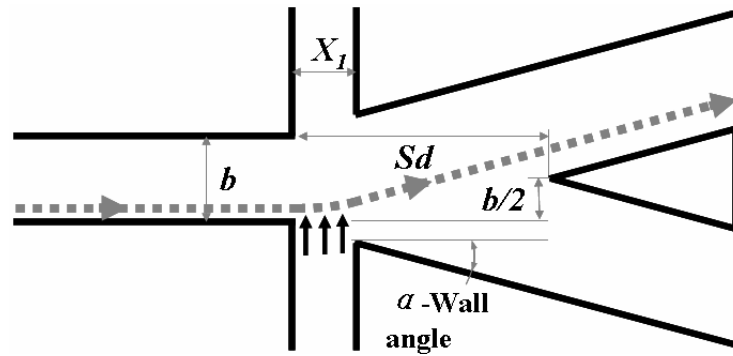


Fig.11: The required vertical translation to completely by-pass the splitter.

The analysis predicts the minimum-switching-pressure in the form:

$$\Delta P_{C,MIN} / \rho U_c^2 > \frac{2b^2}{X_1 Sd - \frac{1}{2} X_1^2}. \quad (3)$$

Interpreting (3) one concludes that larger splitter distance (Sd) and smaller inlet nozzle width (b), while other parameters are kept constant, will reduce the minimum switching pressure.

The maximum pressure, the largest pressure gradient that the valve is able to produce between the control ports when the jet is fully deflected, can be modeled using the same approach. This pressure

gradient is important for creating the self-oscillating condition. The maximum pressure is also the pressure that will cause the jet to attach to the wall at the end of the control ports:

$$\Delta P_{C,\max} / \rho U_c^2 = \frac{b \tan \alpha}{X_1} \quad (4)$$

A larger wall divergence angle (α in Fig.11) requires a larger pressure gradient to reattach. Decreasing the inlet nozzle width (b) or increasing the length of the control region (X_1), with other parameters unchanged, will reduce the maximum pressure. An almost perfect match between the model and the measured minimum and maximum pressures is shown in Fig.16. The minimum switching pressure was measured while the jet was attached to one of the valve walls and the pressure at the control port was increased until the jet flipped to the other side. The maximum pressure was measured while the jet was attached to one of the walls and the two control ports were closed.

This simple theoretical model is able to describe the switching valve operation with satisfactory accuracy, despite all the simplifications, as demonstrated later in the paper by comparing the valve switching model with additional experimental findings.

Jet deflection model results

The model output, as described in the preceding section provides an estimate of the jet deflection at the valve exit. In the experiments, we measured the output *total pressures* using two Pitot pressure probes placed at two fixed points, one at the middle of each valve exit. To convert the model output (deflection) to stagnation pressure, we used Bernoulli's equation $P_0 = 0.5 \rho u^2$. The model assumes that the jet is concentrated at its center line, while the real jet has a finite width. To estimate the output velocity, we assumed that the jet width is that of one output. This enabled us to calculate the flow-rate. By computing the ratio between the jet location and the output width we arrived at the fraction from the maximum flow-rate/velocity that later was converted to pressure using Bernoulli's equation. We also assumed a flat output velocity profile. Since we were interested in switching frequencies, where the switching time from one side to the other is of the same order-of-magnitude as the oscillation period, the effect of the output velocity profile is not significant and the above conversion provides reasonable results.

Figure 12 presents the model input (control pressure, ΔP_c) and output (jet position, y) time-histories. The side-walls and splitter are marked by dashed grey lines. The bi-stable characteristics of the switching valve are clearly seen: the wall-attachment, the rapid switching time and the slope change when the jet approaches the wall (wall attachment effect). The effect of the splitter on the jet deflection is that the jet cannot exit from the region occupied by the splitter and therefore the jet output has a discontinuity at zero deflection.

An option of the computational model was to incorporate the *measured* differential control pressure data as input signal to the model. This yielded a validation of the computational model with the actual valve performance. When this was done, an almost perfect match between the model and the real valve output was found, as shown in Fig.13. The model was able to reproduce a condition when the control pressure was not sufficient for complete wall-attachment. It can be seen that the jet did not reach the lower-wall. The time-delay between input and output, related to the axial transport time (τ), can also be seen in Fig.13. Note that in the measured data it is about twice the axial transport time. This difference can be explained by the simplifying assumption that the jet's axial velocity is constant, i.e., it does not change along the valve due to friction, spreading or entrainment.

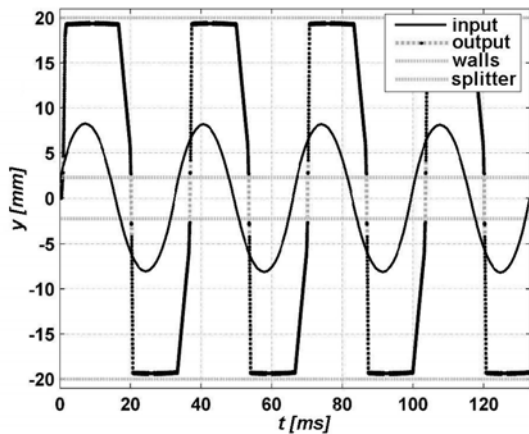


Fig.12: Model input (ΔP_c) and output location time histories for the large-size valve at $P_{in}=160$ kPa.

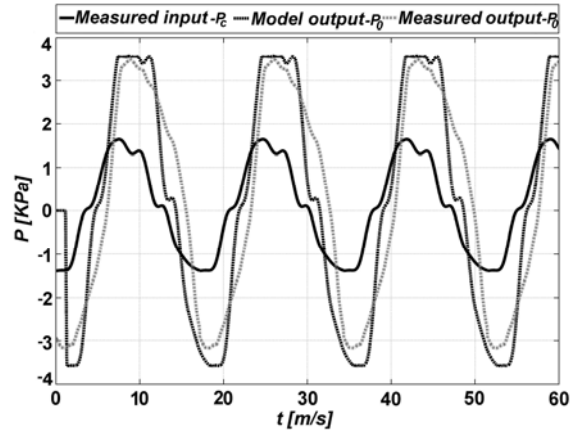


Fig.13: A comparison between experiment and model outputs, for measured input signal. Large-size valve, inlet pressure=80 kPa, input flow-rate=1 liter/sec, $f=58$ Hz. Note that here, the output of the experiment is the exit stagnation pressure.

2.4. Self-excited oscillations frequency model

Several attempts were made in the past to relate the frequency of the self-excited oscillations to the feedback tube volume [22]. Other models attempted to explain the self-excited oscillations mechanism using wave propagation and different combinations of convection and transition times [21,26,27]. None of the models known to the authors was able to predict the frequency for different operating conditions, i.e., feedback tube length and diameter and inlet flow-rate (pressure). Following the current experimental results, a simple model that predicts the self-oscillation frequency was developed and will now be presented and discussed.

Generally, as the valve size decreases, the frequency increases. In addition, one can see in Fig.14a and Fig.14b the basic characteristics of the self-oscillation mechanism from the following experimental observations:

- Oscillation frequency increases with increasing inlet velocity (Fig.14a).
- Frequency decreases with increasing length of the feedback tube (Fig.14b).
- Frequency increases with the tube diameter, for a given tube length (Fig.14b).

It should be taken into consideration that not all the valves can self-oscillate. Geometrical parameters have a strong effect on the ability of the valve to self-oscillate. These will be discussed as we progress with the description of the model and its validation.

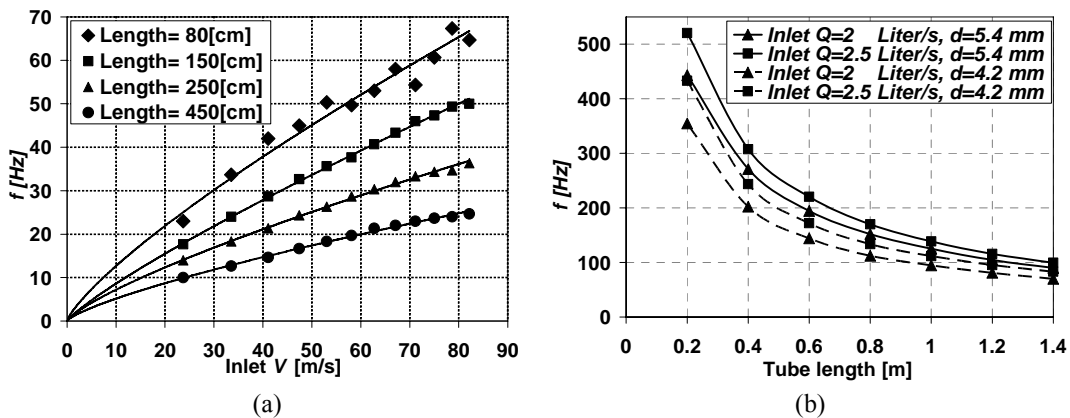


Fig.14: Self-oscillation mechanism basic characteristics. (a) Large-size valve, frequency vs. inlet velocity for different tube lengths, tube diameter=11mm, symbols- experimental data, solid lines-trend lines. (b) Medium-size valve frequency vs. feedback tube lengths for various inlet flow-rates and for two tube diameters.

The self-excited oscillations frequency model is based on two time-scales related to the self-oscillation mechanism and the jet switching mechanism, as exemplified by the electric analogy

presented in Fig.15. Those are the acoustic time delay and the time-constant of an analogous electrical LR (flow inductance-resistance) circuit. In the electrical – fluidic analogy, the inductance, L , represents the fluid inertia and the resistance, R , represents the viscous flow resistance of the feedback tube and the connections between the tube and the valve. The acoustic delay is given by: $\tau_{ac} = \frac{l_t + 2l_c}{a}$, where l_t and l_c are the tube length and the control ports length, respectively. The time constant of an LR circuit is given by $\tau_{LR} = \frac{L}{R}$.

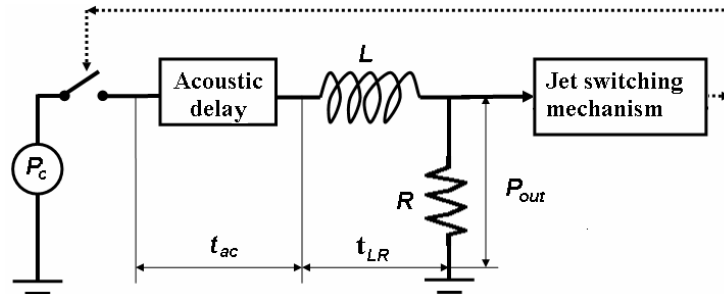


Fig.15: An electric analogy of one-way travel scheme of the self-excited oscillations valve model.

The electrical analogy of fluid systems [28] is given in Table 2 below:

Electrical parameters	Flow parameters
I - current [A]	Q -volume flow-rate [m^3/s]
V -potential [V]	P -pressure [Pa]
R -resistance [Ohm] $R = \frac{V}{I}$ Ohm's law	$R = \frac{P}{Q}$ [$Pa \cdot s/m^3$] = [$kg/m^4 \cdot s$]
L -inductance [Henry] $V = L \frac{dI}{dt}$	$P = L \frac{dQ}{dt}$ [kg/m^4]

Table 2: Electrical analogy of fluid systems [28].

In order to fit the measured data, the resistance R is taken as:

$$R = C \frac{\Delta P_c}{Q} \sqrt{\frac{l_t \cdot d_t}{l_c \cdot d_c}} \quad [Pa \cdot s / (m^3)] \quad (5)$$

The original expression from Table 2 was multiplied by the factor $\sqrt{l_t \cdot d_t}$. Furthermore, in order to retain the proper dimensions the formula was normalized by $\sqrt{l_c \cdot d_c}$, where C in (5) is a dimensionless empirical constant.

The magnitude of the control pressure gradient (ΔP_c) is defined for the stationary jet at one side while the control ports are sealed. It is related to the inlet volume flow-rate by (4) for the small-scale valve (see Fig.16).

Dynamically, the flow-rate cannot instantly rise to its steady-state value (determined by the resistance) because of the inertia effect produced by the flow system "inductance"). The differential equation which describes the rise from zero to its final value is presented along with its electrical analog in parenthesis:

$$P_c = L \frac{dQ}{dt} + QR \quad \left(E = L \frac{dI}{dt} + IR \right) \quad (6)$$

When the control ports are connected, the feedback tube allows this pressure pulse to propagate between the control ports and cause the jet to periodically switch. The minimum steady-state pressure that causes the jet to switch is about $0.3\Delta P_{C,max}$ (Fig.16 and (3)) and the corresponding time-delay is: $t_{LR} = 0.36\tau_{LR}$ (Fig.17).

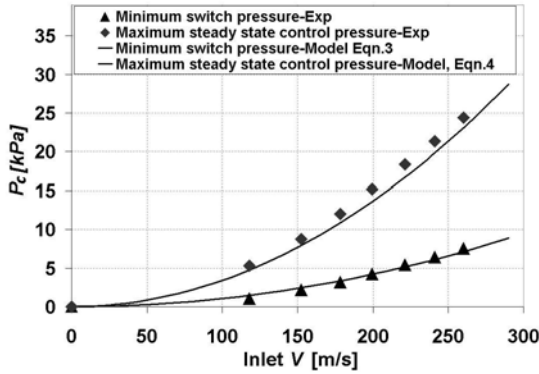


Fig.16: The maximum (P_c) and the minimum switching pressure vs. inlet velocity. For the small-scale valve symbols-experimental data, solid lines-jet deflection model.

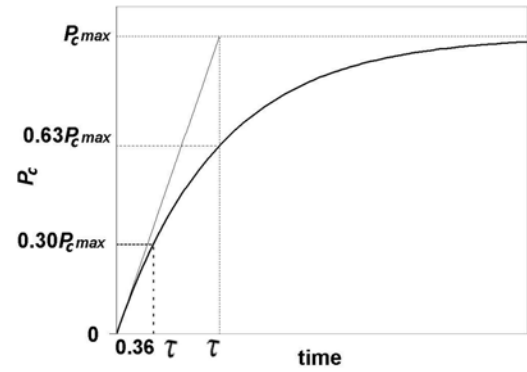


Fig.17: LR circuit time constant and the switching threshold pressure.

Using the above definitions, the self-oscillation frequency is:

$$f = \frac{1}{2(t_{ac} + 0.36\tau_{LR})} = \frac{1}{2 \left(\frac{l_t + 2l_c}{a} + \frac{0.52}{C} \sqrt{\frac{l_c \cdot d_c}{l_t \cdot d_t}} \frac{Q\rho(l_t + l_c)}{AP_c} \right)} \quad (7)$$

The data shown in Fig.18 presents a comparison between the self-oscillation model and the experimental results for the medium and small-size valves. It is evident that the model fits the data very well over a wide range of feedback tube lengths, diameters, and flow-rates for the various size valves.

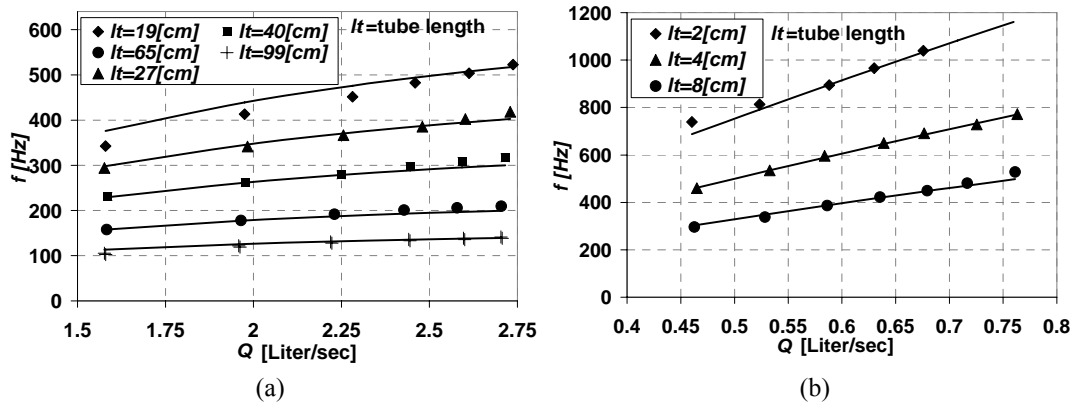


Fig.18: A comparison between the self-excited oscillations model and experimental results for medium and small-scale valves, frequency vs. inlet flow-rate for constant tube diameter and several tube lengths. (a) medium-scale valve (b) small-scale valve.

2.5. Small size ejector

The purpose of the ejector (Fig.4.a) in the new flow control actuator is to create suction flow, increase the flow-rate and inject the flow into the switching valve (Fig.4). The ejector is termed "unloaded" when the main jet is ejected to the free atmosphere without any back-pressure (load). There are two important parameters when testing the unloaded ejector: the flow-rate versus the inlet pressure and the entrainment-ratio ($\eta_e = Q_2/Q_1$), where subscript "2" is the entrained and "1" is the inlet flow-rate, respectively. Figure 19 presents results of small-size ejectors with converging/diverging inlet nozzle. The figure shows the relation between the inlet pressure and the different flow-rates. The total flow-rate is Q_3 .

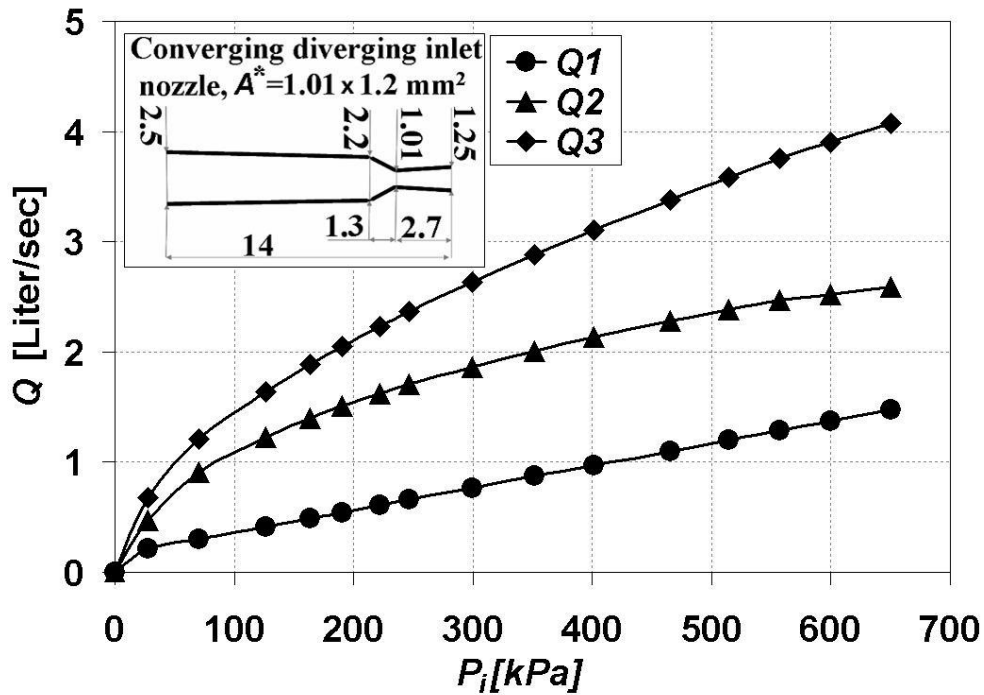


Fig.19: Small-size ejector, unloaded, flow-rates vs. inlet stagnation pressure. Converging-diverging inlet nozzle throat cross section = $1.01 \times 1.2 \text{ mm}^2$.

When the ejector is connected to the valve inlet, it operates against the valve inlet pressure, that is, a back-pressure. Since the ejector efficiency heavily depends on its capability to create low pressure at the suction ports, it is essential to test and optimize the ejector to operate with an exit load (back-pressure).

To increase the ejector's ability to create suction flow, it is necessary to increase the jet energy, for instance, by increasing the jet velocity. Since the ejector's inlet nozzle is small and the inlet pressure is high, ejectors with converging nozzles choke, limiting the jet velocity to the speed-of-sound. To increase the jet velocity, a converging-diverging inlet nozzle was implemented. The nozzle performance can be predicted, assuming isentropic flow conditions [29]. If the flow at the nozzle exit is intended to be supersonic, it is necessary to impose a nozzle pressure ratio that will ensure an ideally expanded jet. A higher pressure-ratio will cause a shock-wave right downstream of the nozzle exit and the flow will return to subsonic conditions.

Figure20 presents a comparison between the performances of several ejector inlet nozzles. Figure20a presents the normalized average exit velocity vs. the back-pressure normalized by the inlet stagnation pressure. As expected, increasing the inlet nozzle cross-section increases the exit

flow-rate. In Fig.20b it can be seen that the entrainment-ratio (Q_2/Q_1 , where Q_2 is the suction flow-rate and Q_1 is the inlet flow-rate) vs. the normalized back-pressure, is superior for the converging-diverging inlet nozzle with a throat cross section of $1.01 \times 1.2 \text{ mm}^2$. By examining the data shown in Fig.20a and Fig.20b, it is concluded that the supersonic flow improves the ejector performance, especially when back-pressure is applied.

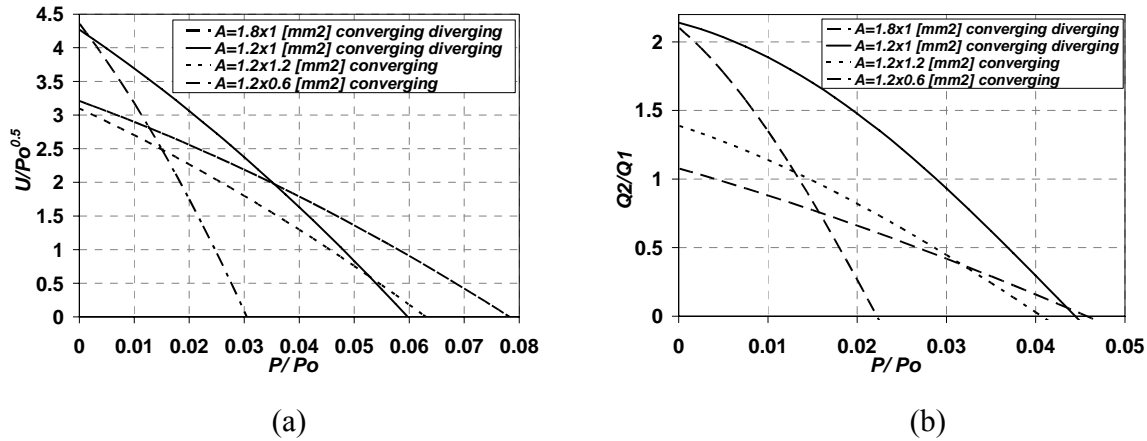


Fig.20: A comparison between several small-size ejectors' inlet nozzles. (a) Average velocity vs. static back-pressure normalized by stagnation pressure (b) Entrainment-ratio (Q_2/Q_1) vs. exit static back-pressure (load) normalized by stagnation pressure

2.6. Improved (4th generation) small-size valve and ejector characteristics

Based on the findings of previous stages of the research, an improved small-size actuator was fabricated. Figure 21 presents data for the 4th generation valve connected to four small-size ejectors. The figure presents the valve flow-rates (inlet shown by solid black line and suction shown by dashed lines) vs. inlet static pressure. The superiority of the ejector with a converging-diverging inlet nozzle and with a throat cross section of $1.01 \times 1.2 \text{ mm}^2$ can clearly be seen. Several operating points for incompressible as well as compressible flow conditions are indicated.

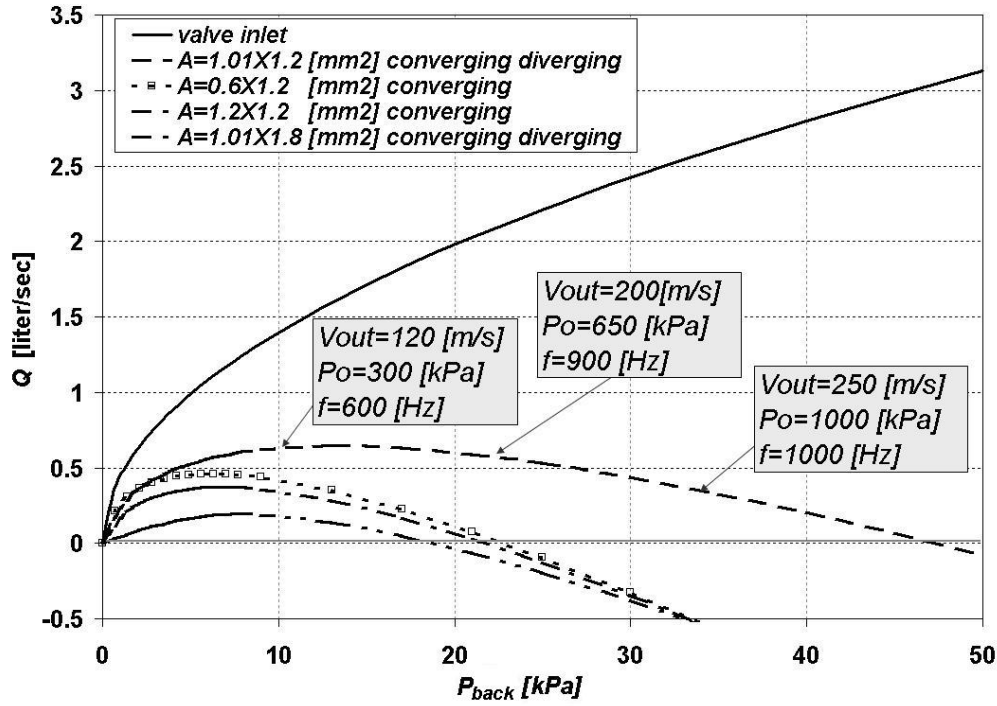


Fig.21: Different ejectors connected to the fourth generation valve, flow-rate vs. back-pressure. Black solid line-valve, dashed lines ejectors suction flow-rate.

2.7. Effectiveness– Overall Figure of Merit

There are many types of flow-control actuators (as briefly reviewed in Section 1 and also by Seifert [30]) with different outputs: velocity fluctuations, unsteady momentum injection, mass removal, vorticity flux and other flow properties. Therefore, comparing their effectiveness is not straightforward.

A candidate actuator effectiveness parameter was suggested in [32], termed Overall Figure of Merit (*OFM*) and defined as:

$$OFM = \frac{F_a^2 U_p}{W_a E} \quad (8)$$

Where W_a is the total weight of the actuation system or of the actuator alone, E is the total actuation system power consumption or just the power delivered to the actuator, U_p is the peak or typical actuator output velocity and F_a is the thrust generated by the actuator when operating in still fluid. Note that the *OFM* is *not* efficiency and therefore, according to its definition, it can reach values that

are greater than unity. A higher *OFM* indicates a *relatively* more effective flow-control device in some sense.

Computing the new actuator effectiveness according the criterion suggested above is not complete, and can essentially estimate only the actuator oscillatory blowing effectiveness. For the suction and oscillatory blowing (SaOB) actuator, $E=Pin*Q$, where the input pressure is measured at a settling chamber upstream of the inlet and the flow rate is calculated from the difference between the output and suction flow rates. If a dedicated system is used to compress air, then its efficiency should be taken into account when calculating E . The effect of the suction is taken by adding the suction momentum to the blowing thrust. This analysis is very conservative, because it is known that steady suction is significantly more effective than steady or pulsed blowing for boundary layer separation control. There is very little data available in the open literature about the effectiveness of suction devices, and certainly not much available regarding the combination of steady-suction and oscillatory-blowing. After more data becomes available, the above assumptions could be revisited.

Figure 22 presents the new actuator *OFM* vs. its peak output velocity. The *OFM* for the new actuator was calculated by adding the suction thrust to the blowing thrust, while the actuator (4th generation) weight was taken as 15g (this weight is based on a device made of aluminum, in future application the actuator can be made from lighter material). For steady-blowing the thrust can be calculated as the momentum flux: $F_a = \dot{m}V = \rho Q^2 / A$. Because the switching valve divides the flow between the two outputs, the thrust was calculated with the area of one output. Moreover, to take into account the possibility of incomplete switching (a situation where the flow rate never reached zero in either exit port) a switching quality factor, $\kappa=Q_L/Q$, is introduced, where the subscript L refers to the left exit, assuming symmetry. This factor can vary between 1 (complete switching) and 0.5 for steady flow being divided equally between the two exit ports. To realistically account for the switching quality, the pulsed blowing part of Eq. 8 should be multiplied by κ^3 . The data shown in Fig. 13 shows a high level of switching quality; $\kappa \approx 0.9$. In future studies, where the valve would be coupled with aerodynamic surfaces this value could be measured more accurately. Currently its value was taken as $\kappa=1$. The power consumption was calculated at the settling chamber as the product of the stagnation pressure and the volume flow-rate.

In Ref. [27], an attempt was made to compare different actuators according to the *OFM*, but very little data is available in the open literature that is required for the calculations of the *OFM* criterion. The information that is provided below is based on conservative evaluations.

The Overall Figure of Merit (*OFM*) compares the actuator performance as it is operated in still air, taking its fluidic output, its weight and power consumption into account. For the actuators used during the XV-15 flight tests and at the flight test conditions [31], the $OFM=0.014$ with $U_p=80.4\text{m/s}$. Comparing this number to those of the TAU developed piezo-fluidic actuators, one finds $OFM=0.052$ [$U_p=20\text{m/s}$, Margalit et al, 5] and $OFM=0.107$ [$U_p=40\text{m/s}$, Timor et al, 32]. For the compact actuator used by Yehoshua and Seifert [$U_p=60\text{m/s}$, 7] the $OFM=0.295$. However, the latest actuator was tested in free-air and was not restricted by installation considerations. Note also the different peak slot velocities in the above comparisons. An estimation of the *OFM* for *DBD* plasma actuators, such as those used by Post and Corke [15] and Goeskel et al. [33], results in $OFM < 1.0 \times 10^{-4}$. This was evaluated for $U_p=3.5\text{m/s}$, a region of influence extending 1mm above the electrode, a total actuator weight of about 4gm/meter and steady-state operation.

It is clear that the new actuator is significantly superior to electro-magnetic and plasma actuators. The latest piezo-fluidic actuator mentioned can deliver 60m/s at $OFM=0.295$. It is estimated that the current actuator can deliver 110 m/s at the same *OFM*.

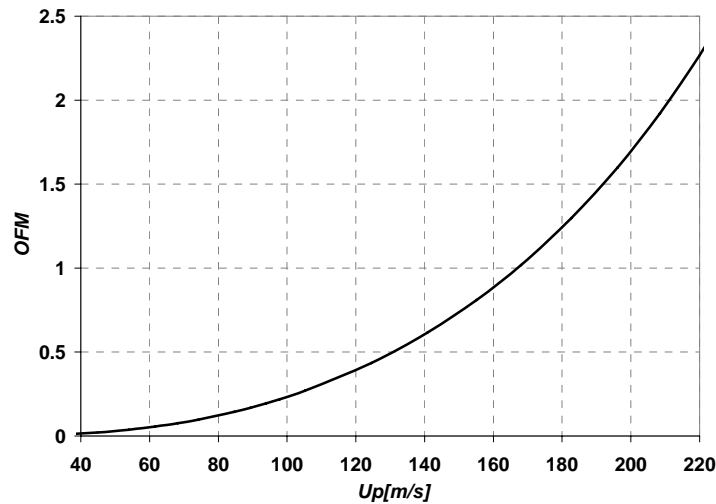


Fig.22: Suction and oscillatory blowing (SaOB) actuator efficiency according to the *OFM* criterion.

According to the *OFM* criterion, the new actuator's effectiveness is superior to and can control much faster flows than other actuators discussed. It is as compact, more robust and as light as the state-of-the-art piezo-fluidic actuators. However, it requires a source of pressurized air and therefore suitable for vehicles operated by jet engines.

3. Conclusions

A new actuator concept, based on the combination of steady-suction and oscillatory-blowing was modeled, designed, fabricated and tested. The new actuator is based on the combination of an ejector and a bi-stable switching valve. The actuator can achieve near-sonic speeds and high operating frequencies that are relevant to compressible flow control applications. It can operate in a self-oscillation mode, therefore requires no control beyond that provided by the inlet flow-rate at a given pressure. Two theoretical models were developed: the *jet deflection model* and the *self-excited oscillations frequency model*. The first model describes the switching-valve operation based on jet deflection between two inclined walls due to a transverse pressure gradient. The second model predicts the oscillation frequency according to the feedback-tube length and diameter, valve inlet flow-rate, and additional empirical relations. The shape of the ejector inlet-nozzle and dimensions were found to be a very important design parameters. A converging-diverging inlet nozzle improves the ejector performance, especially when the actuator is loaded. The ejector was shown to be capable of more than doubling the total mass flow-rate through the actuator. The entrained flow can be sucked into the device from an external or internal boundary layer to be controlled. Detailed static and dynamic tests showed that the actuator is capable of producing the necessary frequencies and amplitudes relevant for active separation control in compressible flows, using also the pulsed flow exiting the switching valve. The new actuator is light, compact, robust and has no moving parts; it therefore provides superior effectiveness and reliability compared to existing actuators.

4. Acknowledgments

The authors would like to thank the following members of the technical staff: Shlomo Moshel, Shlomi Blaivais, Eli Kronish, Mark Vasserman, Avraham Blas and Eli Nevo, for invaluable technical assistance. Special thanks to Shlomo Paster, the laboratory mechanics specialist, for the special efforts undertaken to make the experiments possible. The authors would also like to thank

Assaf Nahum, Eli Ben-Hamou, Oksana Stalnov, Vitalei Palei, Yoni Yom-Tov and Yuri Borisinkov,
our colleagues in the Meadow Aerodynamic Laboratory.

5. References

1. Seifert, A., Greenblatt, D. and Wygnanski, I., "Active separation control: an overview of Reynolds and Mach numbers effects," *Aerospace Science and Technology*, Vol. 8, 2004, pp. 569-582.
2. Seifert, A. and Pack, L.G., "Effects of Compressibility and Excitation Slot Location on Active Separation Control at High Reynolds Numbers", *J. Aircraft* 40, (1): pp. 110-119 Jan-Feb 2003 (part of AIAA paper 2000-0410).
3. Seifert, A., Eliahu, S., Greenblatt, D. and Wygnanski, I., "Use of Piezoelectric Actuators for Airfoil Separation Control (TN)", *AIAA Journal*, Vol. 36, No. 8, 1998, pp. 1535-1537.
4. Amitay, M., Smith, D.R., Kibens, V., Parekh, D.E. and Glezer, A., "Aerodynamic Flow Control Over an Unconventional Airfoil Using Synthetic Jet Actuators", *AIAA Journal*, Vol. 39, No. 3, 2001, pp. 361-370.
5. Margalit, S., Greenblatt, D., Seifert A. and Wygnanski, I., "Delta Wing Stall and Roll Control using Segmented Piezoelectric Fluidic Actuators", (previously AIAA paper 2002-3270), *AIAA J. of Aircraft*, May-June 2004.
6. Cattafesta, L.N. III, Garg, S. and Shukla, D., "The Development of Piezoelectric Actuators for Active Flow Control", *AIAA Journal*, Vol. 39, No. 8, 2001, pp.1562-1568.
7. Yehoshua, T. and Seifert, A., "Boundary Condition Effects on Oscillatory Momentum Generators", *AIAA Paper*, 03-3710, June 2003.
8. Kailasanath, K., "Review of Propulsion Applications of Detonation Waves", *AIAA Journal*, Vol. 38, No. 9, 2000, pp. 1698–1708.

9. Cutler, A.D., Beck, B.T., Wilkes, J.A., Drummond, P.J., Alderfer, W.D., Paul, M. and Danehy, M.P.", Development of a Pulsed Combustion Actuator for High-Speed Flow Control", 43rd AIAA Aerospace Sciences Meeting and Exhibit, Reno, Nevada, AIAA 2005-1084, January 10-13, 2005, pp. 16.
10. Gregory, J. and Sullivan, J., "Characterization of Hartmann Tube Flow with Porous Pressure-Sensitive Paint", AIAA Paper 2003-3713, 33rd AIAA Fluid Dynamics Conference and Exhibit, Orlando, FL, June 23-26, 2003.
11. Ahuja, K.K. and Burrin, R. H., "Control of Flow Separation by Sound", AIAA Paper, 84-2298, Oct. 1984.
12. Kastner, J. and Samimy, M., "Development and Characterization of Hartmann Tube Fluidic Actuators for High-Speed Flow Control", AIAA Journal, Vol. 40, No. 10, 2002, pp. 1926-1934.
13. Labergue, A., Leger, L., Moreau, E. and Touchard, G., "Effect of a Plasma Actuator on an Airflow along an Inclined Wall - P.I.V. and Wall Pressure Measurements", Journal of Electrostatics, 10th international Conference on electrostatics 2005 June 15-17 Espoo/Helsinki Finland.
14. Samimy, M., Adamovich, L., Webb, B., Kastner, J., Hileman, J., Keshav, S. and Palm, P., "Development and characterization of plasma actuators for high-speed jet control", Experiments in Fluids, Vol.37, 2004, pp. 577-588.
15. Post, M.L. and Corke, T.C., "Separation control on high angle of attack airfoil using plasma actuators", AIAA Journal, Vol. 42, No. 11, 2004, pp. 2177-2182.
16. Tesar, V., Hung, C. and Zimmerman, W.B. (2005) No-moving-part hybrid-synthetic jet actuator", Sensors and Actuators A 125, 2006, pp. 159-169.

17. Seifert, A. and Pastuer, S., "Method and mechanism for producing suction and periodic excitation flow", US Patent 7055541, filed 2004-09-07, Issued June 6, 2006 (Priority date Oct-03).
18. Ouzzane, M. and Adieus, Z., "Model Development and Numerical Procedure for Detailed Ejector Analysis and Design", Applied Thermal Engineering, p.p. 2337-2351.
19. Sun, D.-W. and Eames, I.W., "Recent Development in the Design Theories and Applications of Ejector - a Review", Journal of the Institute of Energy, Vol. 68, 1995, pp. 65-79.
20. Kirshner, J.M., "Fluid Amplifiers", McGraw-Hill Book Company, 1966.
21. Viets, H., "Flip Flop Jet Nozzle", AIAA Journal Vol.13, 1975, pp.1375-1379.
22. Raman, G., Rice, E.J. and Cornelius, D., "Evaluation of flip-flop jet nozzles for use as practical excitation devices", ASME Journal of Fluids Engineering, Vol. 116, 1994, pp. 508-515.
23. Drzewiecki, T., "The Design of Fluidic Turbulent Wall Attachment Flip-Flops", Fluidic State-of-the-art Symposium, Vol.1, no.1, 1974.
24. Arwatz, G., "Development and Modeling of Suction and Oscillatory Blowing Actuator for Flow Control Applications", Master thesis, Tel-Aviv University, Israel, August 2006.
25. Kirshner, J.M., and Katz, S., "Design Theory of Fluidic Components", Academic Press, New York, 1975.
26. Simoes, E.W., Furlan, R., Pereira, M.T., "Numerical Analysis of a Microfluidic Oscillator Flowmeter Operating with Gases or Liquids", Technical Proceedings of the fifth International Conference on Modeling and Simulation of Microsystems, MSM 2002, San Juan, Puerto Rico.
27. Tippetts, J.R., Ng, H. K., and Royle, J.K., "An Oscillating Bi-stable Fluid Amplifier for Use as a Flowmeter", Fluidics Quarterly, Vol.5, no 1, 1973.

28. Fox, J. A., " Transients flow in pipes, open channels and sewers", Ellis Horwood Limited, 1989.
29. Streeter, V.L., and Wylie, E.B." Fluid Mechanics, First SI Metric Edition, McGraw Hill Ryerson", 1981.
30. Seifert, A., "Closed-loop Active flow control systems: Actuators", Paper presented at the Conference on Active Flow Control, Berlin, September, 2006. To be included in the book of proceedings.
31. Nagib, H.M., Kiedaisch, J.W., Wygnanski, I.J., Stalker, A.D., Wood, T. and McVeigh, M.A., "First-In-Flight Full-Scale Application of Active Flow Control: The XV-15 Tiltrotor Download Reduction", RTO-MP-AVT-111, 2005, see also: http://fdrc.iit.edu/research/docs/MAFC_XV_15_Briefing_Final.pdf
32. Timor, I., Ben-Hamou, E., Guy, Y. and Seifert, A., "Maneuvering Aspects and 3D Effects of Active Airfoil Flow Control", AIAA paper 2004-2614, June, 2004. J. Flow, Turb and Comb., to be published.
33. Göksel, B. and Rechenberg, I., " Active Separation Flow Control Experiments in Weakly Ionized Air". In Andersson H. I. and Krogstad P.-Å. (eds.) Advances in Turbulence X, Proceedings of the 10th Euromech European Turbulence Conference, CIMNE, Barcelona, 2004.